LANGMUIR Article
Cite This: Langmuir 2018, 34, 12310−12317
pubs.acs.org/Langmuir

Kinetic Insights into Marangoni Effect-Assisted Preparation of Ultrathin Hydrogel Films

Ye Tian,[†] Xiaoying Gao,[†] Wei Hong,[*,‡,§,∥] Miao Du,[†] Pengju Pan,[⊥] Jing Zhi Sun,[†] Zi Liang Wu,[*,†] and Qiang Zheng[†]

[†]Ministry of Education Key Laboratory of Macromolecular Synthesis and Functionalization, Department of Polymer Science and Engineering, [§]Department of Engineering Mechanics, and [⊥]State Key Laboratory of Chemical Engineering, College of Chemical and Biological Engineering, Zhejiang University, Hangzhou 310027, China

[‡]Department of Mechanics and Aerospace Engineering, Southern University of Science and Technology, Shenzhen 518055, China

[∥]Global Station for Soft Matter, Global Institution for Collaborative Research and Education, Hokkaido University, Sapporo 060-0810, Japan

Supporting Information

ABSTRACT: In a previous work (*ACS Appl. Mater. Interfaces* **2017**, *9*, 34349−34355), a facile approach was reported to prepare thin hydrogel films based on the Marangoni effect. After dripping onto a water surface, a drop of ethanol solution of poly(stearyl acrylate-*co*-acrylic acid) [P(SA-*co*-AAc)] spread quickly to form a thin film. The solvent exchange from ethanol to water led to the gelation of polymer solution which turned into a hydrogel film. Here, we investigate the scenario and seek for the governing kinetics of the Marangoni effect-assisted preparation of hydrogel films. By incorporating aggregation-induced emission fluorogens into the P(SA-*co*-AAc) solution, so that fluorescence appears at the gel state, we found that the spreading usually completed before the full gelation of the entire film. The spreading and formation of the gel films were influenced by the molar fraction of SA, *f*, and the polymer concentration of ethanol solution, C_P. The spreading was blocked when C_P was too high, whereas the film was fragmented into small pieces when C_P was too low. At an intermediate C_P, uniform hydrogel films were obtained. Steady spreading at a constant speed was observed during the processes which yielded uniform hydrogel films. Both C_P and *f* influenced the spreading process by tuning the surface tension of the ethanol solution and the viscoelasticity of the gelated film, as suggested by our theoretical model. This work provided kinetic insights into the Marangoni phenomena of viscous polymer solutions. The strategy and principle should be applicable to other systems on preparing thin supramolecular gel films with versatile functions.

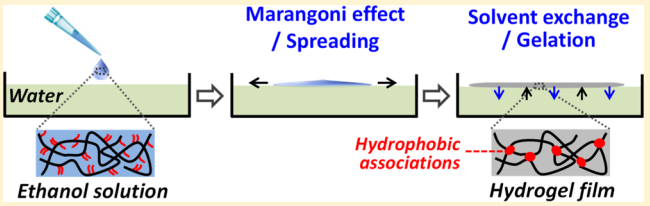

INTRODUCTION

Hydrogel films, as a type of low-dimensional smart materials, have attracted tremendous attention because of their promising applications in wound dressing, soft actuators, surgical diaphragms, and so forth.[1−4] The gel films are usually prepared by solution casting and spin-coating, followed by a physical or chemical gelation process.[5−7] For example, Aoyagi et al. have prepared hydrogel films with nanometer-scaled thickness by spin-coating a photocrosslinkable polymer solution of poly(*N*-isopropylaclylamide-*co*-2-carboxyisopropylaclylamide) and subsequently crosslinking it under UV irradiation.[5] However, it is challenging to handle such ultrathin hydrogel films because of their poor mechanical properties, which also greatly limited their applications. There is an urgent demand for tough hydrogel films developed through facile approaches.

In recent years, various tough hydrogels have been developed by controlling the network structures and incorporating energy-dissipating mechanisms.[8−11] These achievements have paved the way to design ultrathin tough hydrogel films.[12−17] For instance, Shull et al. developed tough physical hydrogel films with a thickness of several hundred micrometers by solution casting of an ABA-type triblock polymer [A: poly(methacrylic acid) (PMAA); B: poly(methyl methacrylate) (PMMA)] and subsequently swelling the dry film in a solution of divalent metallic ions, in which the PMMA blocks segregated to form nanometer-sized hydrophobic domains and PMAA blocks were crosslinked by the metallic ions.[14] The resultant hydrogel films possessed excellent mechanical properties including a tensile strength of 0.4−1 MPa and a breaking strain of 100−500%. However, a precise control of thickness and uniformity of the hydrogel films remained challenging.

Recently, a facile approach based on the Marangoni effect was reported to prepare ultrathin and tough physical hydrogel films.[18] After dripping onto water, a drop of ethanol solution of

Received: August 2, 2018
Revised: September 20, 2018
Published: September 21, 2018

DOI: 10.1021/acs.langmuir.8b02626
Langmuir 2018, 34, 12310−12317

poly(stearyl acrylate-*co*-acrylic acid) [P(SA-*co*-AAc)] rapidly spread to form a thin film. The solvent exchange from ethanol to water led to the segregation of the long alkyl chains of SA units to form hydrophobic domains that served as the physical crosslinking junctions of the hydrogel.[19,20] The spreading was driven by the huge difference in surface tension between ethanol and water, whereas the gelation was triggered by the spontaneous solvent exchange. However, the detailed process and the interplay among the different physical processes remained unclear. In addition, the influences of the polymer composition and the concentration of ethanol solutions on the spreading/gelation process have not been explored. A systematic study is required to address these issues and thus merit designing other thin films with desired properties.

We present here a combined experimental and theoretical study, which provided kinetic insights into this Marangoni effect-assisted preparation of ultrathin physical hydrogel films. A morphological phase diagram was obtained by varying the polymer concentration of ethanol solution, C_P, and the SA fraction of the copolymer, f. The spreading was blocked when C_P was too high, whereas the film was fragmented into small pieces when C_P was too low. At an intermediate C_P, unbroken hydrogel films were formed, yet uniform films were only obtained at a relatively high C_P; otherwise, the gel films showed a gradient thickness. In addition, the spreading process, including the spreading distance and speed, was analyzed from the videoclips. The influences of C_P and f on gel morphologies were studied in terms of solution viscosity and surface tension, both of which would affect the spreading process and ultimately film morphology. By incorporating aggregation-induced emission (AIE) fluorogens, which were only lit in a gel state, we found that the spreading was usually completed much earlier than the gelation process. Through a continuum model, considering solvent diffusion, solution viscosity, and the elasticity of the gel film, we rationalized the observations and identified the key mechanism for the steadiness and uniformity of the spreading: the formation of a thin gel membrane at the solution−water interface.

EXPERIMENTAL SECTION

Materials. SA (Tokyo Chemical Industry Development Co., Ltd.) and 2,2′-azobis(isobutyronitrile) (AIBN, Sigma-Aldrich) were recrystallized from ethanol. AAc (Aladdin Industrial Corporation) was purified by vacuum distillation at 90 °C. Ethanol (Sinopharm Chemical Reagent Co., Ltd) and rhodamine B (Aladdin Industrial Corporation) were used as received. The AIE fluorogen, 1,2-bis(4-(2-bromoethoxy)phenyl)-1,2-diphenylethene, was synthesized according to the literature.[21] Millipore deionized water was used in all the experiments.

Synthesis of Copolymers. P(SA-*co*-AAc) with various molar fractions of SA, f, was synthesized by free-radical copolymerization of SA and AAc in ethanol, with AIBN as the initiator. The chemical structure of P(SA-*co*-AAc) is shown in Figure 1a. The resulting product was precipitated in ether and dried at 50 °C to obtain solid P(SA-*co*-AAc).

Preparation of Gel Films. A prescribed amount of P(SA-*co*-AAc) was dissolved in ethanol to form a transparent solution with a certain concentration of the copolymer, C_P. Then, one droplet of the ethanol solution with a specified volume was dripped onto water. The ethanol solution spread quickly to form a thin film on the water surface. The subsequent solvent exchange from ethanol to water resulted in gelation to form a physical hydrogel film. The hydrogel film containing AIE fluorogens was prepared in a similar way. A drop of dimethylformamide (DMF) solution of P(SA-*co*-AAc) with a small amount of AIE fluorogens was dripped onto water. The spreading and gelation processes were observed under an irradiation of 365 nm UV light.

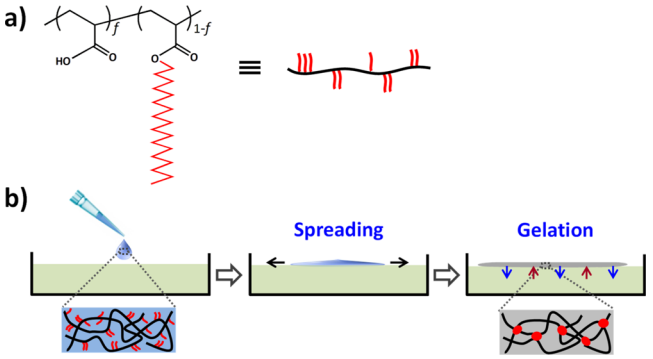

Figure 1. Molecular structure of P(SA-*co*-AAc) (a) and schematic illustration of the preparation of hydrogel films (b).

Characterizations. The spreading process to prepare a hydrogel film was recorded by a digital camera. A 0.2 wt % of rhodamine B was added to the ethanol solution of P(SA-*co*-AAc) for visualization. The variations of the film diameter with the spreading time were analyzed with an image data analyzer (Potplayer) from the recorded video. The thickness profile of the hydrogel film was examined by a digital stereomicroscope (VH-Z100R, Keyence Corporation). The gel film was transferred from the water surface onto a glass substrate for microscope observation. The thickness profile at specific locations of the gel film was obtained by scanning the upper and bottom surfaces of the gel film; the distance between the two focus planes was the local thickness. The thickness profile was obtained by measuring the thickness at a series of locations along the diameter of the disk gel film. The surface tension and viscosity of the ethanol solution of copolymer were measured at room temperature by using an optical dynamic/static interfacial tensionmeter (Dropmeter, MAIST Vision Inspection & Measurement Co., Ltd.) and a rheometer with a parallel plate setup (ARG-2, TA), respectively. The fluorescence spectra of the DMF solution and the corresponding gel film containing AIE fluorogens were obtained using a RF-5301PC fluorescence spectrometer (Shimadzu).

RESULTS AND DISCUSSION

As shown in Figure 1b, the hydrogel films were facilely prepared by dripping one drop of the ethanol solution of P(SA-*co*-AAc) onto water. Because of the huge difference in surface tension between water and ethanol (72 and 22 mN/m, respectively, at 25 °C),[22,23] the ethanol solution quickly spread to form a thin film on the water surface; this phenomenon is termed as Marangoni effect,[24,25] which has been widely used for the designing of self-propel and chemomechanical systems.[26−31] Meanwhile, solvent exchange from ethanol to water occurred within the film, resulting in the hydrogelation of the copolymer, in which the long alkyl chains of the SA units segregated to form hydrophobic domains acting as physical crosslinks.[19,20]

Apparently, the spreading and gelation processes are associated with the copolymer concentration of ethanol solution, C_P, and the molar fraction of SA in the copolymer, f, both of which influence the surface tension, viscosity, and gelation kinetics of the ethanol solution. The morphologies of the gel films prepared with different C_P and f are summarized in a phase diagram (Figure 2a). As C_P decreased, the resulting samples changed from blocked thick gels to films of uniform or gradient thickness and then to cracked films or fragmented pieces (Figure 2b). For example, the spreading of ethanol solutions with f = 8 mol % and C_P > 43 wt % was blocked

DOI: 10.1021/acs.langmuir.8b02626
Langmuir 2018, 34, 12310−12317

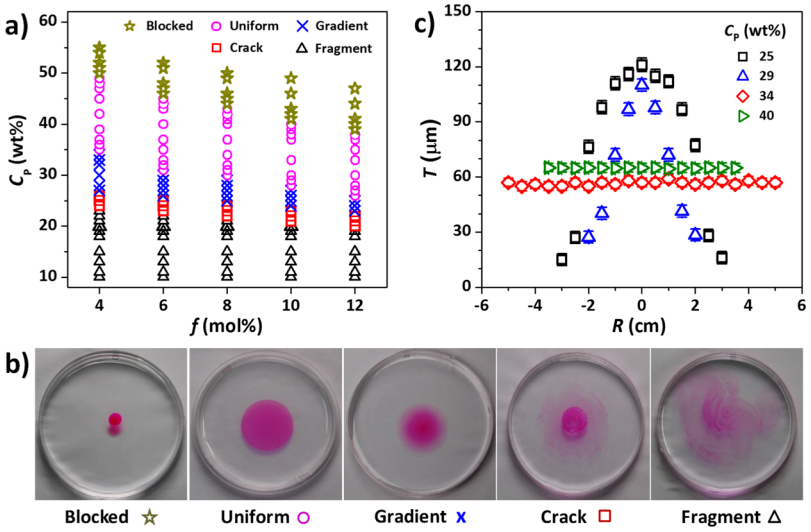

Figure 2. (a,b) Morphological phase diagram of samples with different fractions of SA and polymer concentrations (a) and representative morphologies (b). (c) Thickness profiles of hydrogel films prepared with different polymer concentrations, C_P. T and R are the thickness and the distance from the center of the disk gel film, respectively. The fraction of SA, f, and the volume of the polymer solution, V_P, are 8 mol % and 60 μL, respectively.

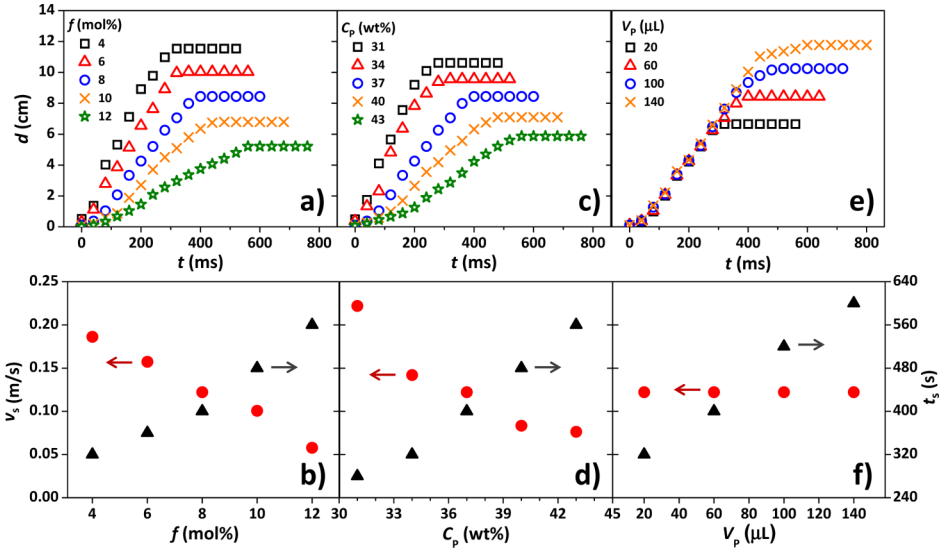

Figure 3. Variations of film diameter, d, as a function of spreading time, t (a,c,e), and the corresponding steady spreading speed, v_s, and the terminal time of spreading, t_s (b,d,f). (a,b) Different f, C_P = 37 wt %, V_P = 60 μL; (c,d) different C_P, f = 8 mol %, V_P = 60 μL; and (e,f) different V_P, f = 8 mol %, C_P = 37 wt %.

because of the relatively high viscosity and surface tension in the solutions, corresponding to the high resistance and low driving force for spreading. When C_P decreased in the range of 30−43 wt %, hydrogel films with uniform thickness were obtained (Figure 2c), indicating a balance between the resistance and the driven force for spreading. As expected, the thickness of the gel films increased, whereas the diameter decreased with an increase in C_P.[18] However, gel films with gradient thickness were formed when 24 wt % < C_P < 30 wt %. A further decrease in C_P led to the fragmentation of the samples. This was caused by a relatively fast gelation and loss of deformability in the gel film, which was torn apart by the surface tension. As C_P decreased further, no integrated gel films were obtained. A few cracks were observed at the edge of the gel films when 21 wt % < $C_P \leq$ 24 wt %, whereas the gel films were broken into small pieces when $C_P \leq$ 21 wt %.

The spreading and gelation processes were also influenced by the SA fraction of the copolymer, f. As shown in Figure 2a, as f increased, the boundary between the different states shifted to low C_P. However, uniform hydrogel films can be obtained over a wide range of C_P and f.

To reveal the spreading process in detail, variations of the film diameter, d, with the spreading time, t, were analyzed from the recorded movies. As shown in Figure 3a, d almost increased linearly with t until the spreading ceased. The steady-state spreading speed, as calculated from the half slope of the linear region, decreased from 0.19 to 0.06 m/s, with the increase in f from 4 to 12 mol %. The spreading speed is determined by the ratio between the differential surface tension as the driving force and the viscosity of the solution. The low f corresponded to a relatively large driven force and a low resistance, which led to a relatively high spreading speed, v_s

DOI: 10.1021/acs.langmuir.8b02626
Langmuir 2018, 34, 12310−12317

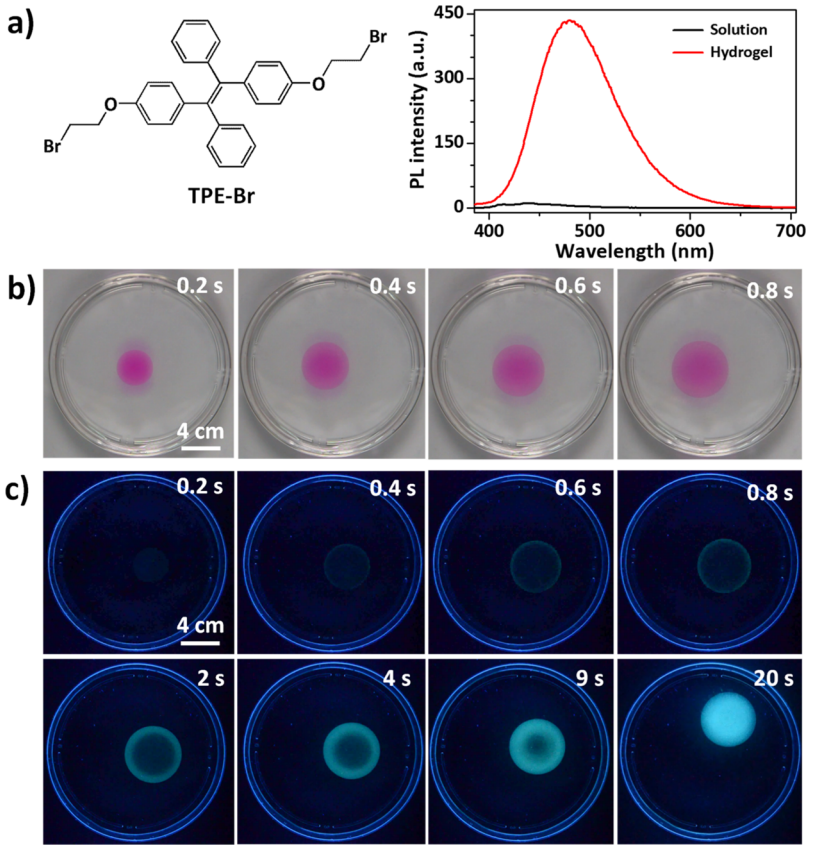

Figure 4. (a) Molecular structure and photoluminescence spectra of the AIE fluorogen in the DMF solution of P(SA-*co*-AAc) and the corresponding hydrogel after solvent exchange. (b,c) Spreading process of the DMF solution of P(SA-*co*-AAc) containing rhodamine B under daylight (b) and AIE fluorogen under UV radiation (c). f = 10 mol %, C_P = 37 wt %, V_P = 60 μL; the contents of rhodamine B and AIE fluorogen are 0.2 and 0.01 wt % of the DMF solution, respectively.

(Figure 3b). In the meanwhile, the faster spreading led to a larger film before the gelated part became too stiff to be further spread, and the process was completed at a shorter time, t_s (Figure 3a). The effect of C_P on the spreading speed was similar to that of f. As shown in Figure 3c,d, v_s decreased with the increase in C_P; higher C_P resulted in a longer t_s of the spreading and a smaller d of the gel film. We should note that the spreading at the initial stage was nonlinear, especially at the systems with high f or high C_P (e.g., f = 12 mol % in Figure 3a and C_P = 43 wt % in Figure 3c). The initial acceleration stage was expected to be due to the shear-thinning rheology: the increase in spreading speed decreased the viscosity of the ethanol solution until the steady spreading (Figure S1). The systems with high f or high C_P had a relatively high viscosity and a low driven force and thus needed a longer acceleration time. In the systems with low f or C_P, the acceleration stage should also exist, albeit short. As shown in Figure 3e,f, the volume of the ethanol solution, V_P, did not influence the spreading speed. The variations of the film diameter with the spreading time for the systems with different V_P almost overlapped with each other because of the same dynamic resistance and driven force for spreading. As expected, the final diameter, d, increased with the volume of the polymer solution, V_P. However, there should be an upper limit of V_P to form the uniform hydrogel films.

The spreading process was driven by the Marangoni effect, associated with a vigorous solvent exchange between ethanol and water, resulting in the hydrogelation of the P(SA-*co*-AAc) solution. The coupling of spreading and gelation makes the kinetics more complicated, as will be discussed in the following section. We noticed that spreading was completed within 0.6 s (Figure 3). On the other hand, with the relatively low diffusion coefficient, ~1 × 10^{-9} m^2/s,[32,33] the water molecules could only penetrate a thin layer across the original solution−water interface, when the thickness of the drop was greatly reduced by the spreading process. During the spreading process, the P(SA-*co*-AAc) solution film should not be fully gelated, yet a thin gel layer might be produced at the interface. The hypothesis that the spreading is completed ahead of the gelation process was confirmed by observing the gelation process of the P(SA-*co*-AAc) solution containing AIE fluorogens as dopants. The AIE fluorogen, 1,2-bis(4-(2-bromoethoxy)phenyl)-1,2-diphenylethene (TPE-Br), was soluble in DMF, yet insoluble in water (Figure 4a).[21] The fluorescent probe was only lit in a gel matrix, where the intermolecular motions were restricted and thus led to fluorescence emission.[34,35] As shown in Figure 4b,c, one drop of DMF solution of P(SA-*co*-AAc) containing the fluorogens dripped onto water and quickly spread to form a thin film. This film was not fluorescent under a 365 nm UV irradiation, indicating that the film is mainly in a solution state. However, the film gradually became fluorescent with time, indicating that the gelation process was completed after the spreading. It is interesting that the gelation occurred from the edge to the center of the uniform thin film, suggesting that the solution at the edge of the uniform thin film was exposed earlier to water and thus gelated ahead of the central part.

DOI: 10.1021/acs.langmuir.8b02626
Langmuir 2018, 34, 12310−12317

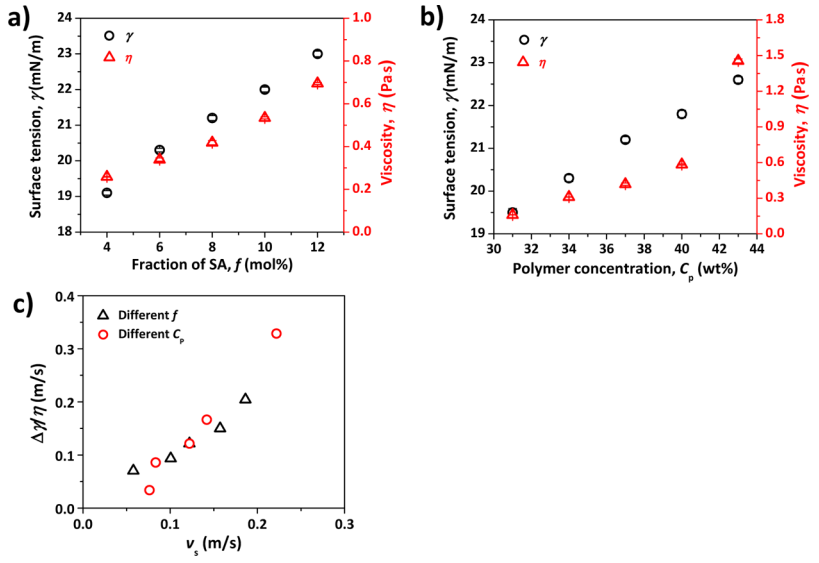

Figure 5. (a,b) Variations of surface tension and viscosity of the ethanol solution of P(SA-*co*-AAc) as a function of fraction of SA, f (a), and polymer concentration, C_P (b) at room temperature. (a) Different f, C_P = 37 wt %, V_P = 60 μL; (b) different C_P, f = 8 mol %, V_P = 60 μL. (c) Plot of $\Delta\gamma/\eta$ vs v_s for the systems with different f and C_P.

The spreading process with a constant speed was quantitatively analyzed in terms of differential surface tension and dynamic viscosity, respectively. The differential surface tension $\Delta\gamma$ is defined as $\Delta\gamma = \gamma_w - \gamma_s$, in which γ_w and γ_s are the surface tensions of water and ethanol solution of copolymer, respectively. At room temperature, γ_w was 72 mN/m, and γ_s increased from 19.1 to 23.0 mN/m as f increased from 4 to 12 mol %, or increased from 19.5 to 22.6 mN/m as C_P increased from 31 to 43 wt % (Figures 5a,b and S2). As a consequence, $\Delta\gamma$ decreased with the increase in f or C_P. The variations in the viscosity of the ethanol solutions, η, showed the similar tendency; at room temperature, η increased from 0.26 to 0.69 Pa·s as f increased from 4 to 12 mol %, or increased from 0.16 to 1.45 Pa·s as C_P increased from 31 to 43 wt %. The ratio between the dynamic viscosity of the P(SA-*co*-AAc) solution η and the differential surface tension $\Delta\gamma$ defines a velocity, which is expected to scale with the spreading velocity[36]

$$v_s \approx \frac{\Delta\gamma}{\eta} \tag{1}$$

This scaling relation was confirmed by the experimental results for the P(SA-*co*-AAc) solutions with various f and C_P, as shown by Figure 5c, indicating that the differential surface tension and viscous stress are indeed the dominating driving force and the rate-limiting mechanism, respectively.[37]

Despite the good agreement between the experiments and the scaling law of eq 1, the detailed process was unclear. The observations in the current system including the gelation process contradicted the existing theories of Marangoni effect-driven spreading: a Newtonian fluid drop does not spread at a constant speed, and the localized surface tension should result in a highly nonuniform film.[38−42] To rationalize the observations, we hypothesized the following spreading and gelation processes. Even though the complete gelation took a relatively long time, the solvent exchange near the drop−water interface was very fast, leading to a thin elastic (or highly viscous) gel layer enclosing the remaining liquid solution, as shown schematically by Figure 6. A piece of evidence of such a

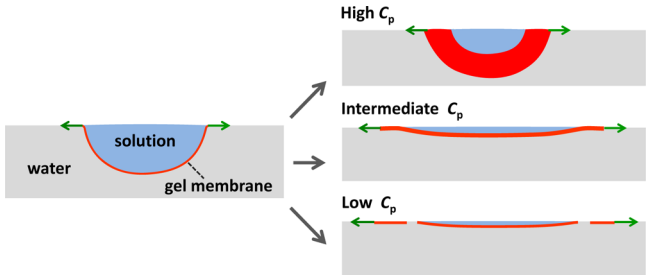

Figure 6. Sketch of the spreading and gelation processes under various polymer concentrations.

thin layer was the fragmented films at a relatively low copolymer concentration, C_P (Figure 2b), resulting from the gel film formed at an early stage and later torn apart by the Marangoni force, as a film of liquid solution is unlikely to be fractured into smaller pieces with sharp and relatively straight boundaries. After the formation of the elastic membrane, the force due to the differential surface tension was exerted over its edge rather than the liquid solution. As the membrane was very thin and flexible, it provided almost no resistance to the spreading until it was flattened. The speed of spreading was still limited by the viscosity of the enclosed solution. At a relatively high C_P, both the viscosity of the bagged fluid and the stiffness of the membrane were high, preventing the drop from spreading before significant gelation. At a relatively low C_P, the softer membrane and less viscous fluid enabled very fast spreading, whereas the membrane was still thin and could not withstand the differential surface tension and was ultimately torn apart. Only an intermediate C_P allows effective spreading and a thick enough gel membrane against tearing when flattened, leading to a uniform and continuous gel film. It is noteworthy that the membrane grew in thickness throughout the entire process. To further elucidate the process, a numerical model accounting for mass transportation, viscous flow, and elastic deformation was established as follows.

For simplicity, we will neglect the shear-thinning effect and focus only on the steady-state spreading. The ethanol solution of P(SA-*co*-AAc) is modeled as an incompressible Newtonian

DOI: 10.1021/acs.langmuir.8b02626
Langmuir 2018, 34, 12310−12317

fluid with viscosity η, and the viscous Cauchy stress σ^{v} is proportional to the symmetric part of the velocity gradient

$$\sigma_{ij}^{v} = \frac{\eta}{2}\left(\frac{\partial v_i}{\partial x_j} + \frac{\partial v_j}{\partial x_i}\right) \tag{2}$$

In eq 2 and the following equations, the indices, for example, i and j, represent the Cartesian components of tensors and vectors, and the repeated indices indicate a summation over all spatial dimensions, following Einstein's convention. Given the size of the drop and the viscosity, the Reynolds number of the flow is relatively low. Using a typical velocity ~0.2 m/s and a viscosity ~0.2 Pa·s, we estimate the Reynolds number of a spreading film of thickness 100 μm to be ~0.1. We therefore neglect the inertia and assume a static mechanical equilibrium in the solution:

$$\frac{\partial \sigma_{ij}}{\partial x_i} = 0 \tag{3}$$

The actual physical process involves the interdiffusion between the two solvents, ethanol and water. Here, the process is simplified into a Fickian diffusion equation of normalized water concentration C

$$\frac{\partial C}{\partial t} = D\frac{\partial^2 C}{\partial x_i \partial x_i}, \tag{4}$$

where D is the effective diffusivity. The normalized concentration varies from $C = 0$ in the initial ethanol solution to $C = 1$ in the state in equilibrium with water.

After water diffuses in, gelation takes place, and the polymer solution transforms from a viscous fluid into a viscoelastic solid. The rheology of the viscoelastic gel during formation, however, is almost impossible to be measured. As suggested by the experimental results, the spreading is directly correlated to the solution viscosity. Thus, we neglect the viscosity of the gel membrane and model it as a neo-Hookean solid with the elastic Cauchy stress

$$\sigma_{ij}^{e} = \mu F_{iK} F_{jK} \tag{5}$$

where $F_{iK} = \partial x_i/\partial X_K$ is the deformation gradient that links the current coordinate x of a material particle to its coordinate X in the reference state. We further assume the shear modulus μ to be proportional to the normalized water concentration C: $\mu = \mu_0 C$, with μ_0 being the shear modulus of the fully gelated state. Combining the two stress contributions in eqs 2 and 5 and substituting the total Cauchy stress $\sigma = \sigma^{v} + \sigma^{e}$ into eq 2, we obtain a partial differential equation for the field of displacement. The material is assumed to be incompressible, and the constraint $\det \boldsymbol{F} = 1$ is enforced by using a Lagrange multiplier.

The coupled mechanical equilibrium and diffusion equations are solved numerically in the domain of the solution droplet, which is assumed to be hemispherical in the initial state, by using a commercial finite-element package, COMSOL Multiphysics 5.2. It is further assumed that the geometry and the evolution of the system are axisymmetric; thus, only the cross-section is modeled, as sketched in Figure 7. As the viscosity of water is much lower than that of the copolymer solution, the flow in the surrounding water is not included in the model, and the viscous force on the interface is neglected. The solution–water interface is taken to be stress-free. We also assume neutral buoyancy, so that the top surface of the solution

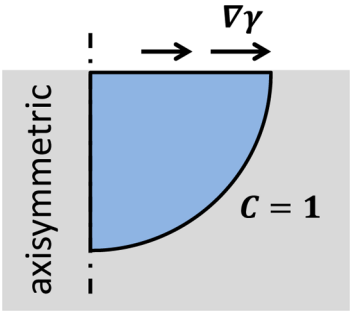

Figure 7. Sketch of the geometry and boundary conditions of the model, and the axisymmetric cross section of a hemispherical domain in the initial stage. The solution–water interface is set to be traction-free, and the normalized water concentration is set to be $C = 1$. The top surface is constrained to be flat, with the effect of surface tension gradient modeled as a distributed tangential force.

remains horizontal and flat. The Marangoni effect is modeled by a distributed tangential force on the top surface, $\tau = \nabla\gamma = d\gamma/dC\ \nabla C$.[43] We further assume a linear dependence of surface tension on the normalized water concentration, $\tau = \Delta\gamma\nabla C$. As a boundary condition for the diffusion equation, the normalized concentration $C = 1$ is prescribed on the interface. With these boundary conditions, the coevolution of the concentration and deformation can be readily calculated. A representative deformed shape of the droplet in the early stage of spreading is shown in Figure 8a. The Marangoni force is

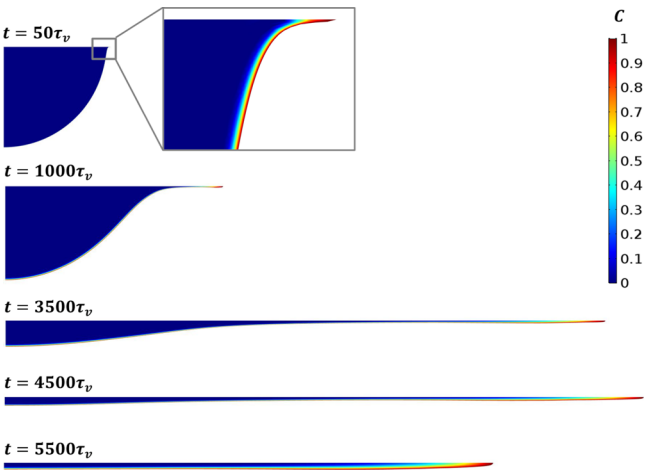

Figure 8. Snapshots of the spreading process of a hemispherical drop of the copolymer-ethanol solution. The color scale indicates the normalized water concentration C. The region of higher water concentration is modeled as an elastic gel.

concentrated at the top surface on the ethanol–water interface, resulting in a highly localized deformation, which further leads to the spreading of the copolymer solution into a thin layer around the perimeter. The diffusion creates a thin layer of polymer gel near the ethanol–water interface. This thin gel layer provides an elastic force and stabilizes further deformation localization.

A representative spreading process predicted by the model is shown by Figure 8. Initially, the droplet is entirely fluid. The Marangoni force is concentrated at the rim of the droplet, causing a highly localized deformation and spreading a very thin layer of liquid film. The liquid film thickness scales with the characteristic length $L_v = \eta D/\Delta\gamma$. Taking the representative

DOI: 10.1021/acs.langmuir.8b02626
Langmuir 2018, 34, 12310–12317

values $\eta \approx 0.5$ Pa·s, $\Delta\gamma \approx 50$ mN/m, and D $\approx 10^{-9}$ m^2/s, the characteristic length is estimated to be on the order of $L_v \approx 10$ nm. Obviously, such a small length is not directly related to the dimension of the gel film experimentally obtained. Indeed, this initial stage only lasts for a very short time (with the characteristic time $\tau_v \approx D(\eta/\Delta\gamma)^2 \approx 0.1$ μs), after which the drop is diffused with water and forms a gel membrane. With the gel elasticity sharing a major part of the Marangoni load, the liquid drop thickens and further spreads. Because of the membrane tension in the elastic gel film, the entire drop is being compressed more uniformly, in contrast to the very localized spreading in the initial stage. At the same time, as water diffuses deeper into the liquid drop, the gel membrane also grows in thickness. If the gel membrane maintains its integrity and is not too stiff, the entire drop will be flattened into a film with very uniform thickness and solidified via gelation. The ultimate film thickness is determined by another characteristic length, $L_e = \Delta\gamma/\mu_0$. Taking the typical thickness of the gel film prepared in the experiments, $L_e \approx 60$ μm, we could estimate the stiffness of the hydrogel to be $\mu_0 \approx 1$ kPa. We may also estimate the time of spreading from the time of water diffusion through the film, $\tau_e = L_e^2/D = \Delta\gamma^2/\mu_0^2 D \approx 3$ s, which is comparable to the observed time of spreading.

One shortcoming of the current model is the stress-free reference state of the gel film. The simple neo-Hookean model assumes the initial hemispherical geometry to be at the stress-free state, whereas the gel film formed during the spreading process would likely be stress-free at the as-gelated state. Such a discrepancy affects the behavior of the gel film after flattening—its elasticity tends to pull it back to the initial stress-free state, as shown by the last snapshot of Figure 8—whereas the actual gel film showed no significant retraction after spreading.

The ratio between the two length scales defines a dimensionless material parameter, $\mathcal{M} = L_v/L_e = \sqrt{\tau_v/\tau_e} = \mu_0\eta D/\Delta\gamma^2$, which characterizes the elastic resistance against the Marangoni spreading. The growth in radius (the spreading displacement) at various values of the parameter $\mathcal{M}$ is shown in Figure 9. At a relatively high $\mathcal{M}$, the elasticity of the gel membrane dominates, and the drop hardly spreads before full gelation (the case of high C_P). At an intermediate $\mathcal{M}$, the drop spreads steadily, resulting in a uniform gel film. At a relatively low $\mathcal{M}$ (the case of low C_P), the model shows that the gel spreads very fast, resulting in a very large film. However, the large extension in the gel film may exceed the stretch limit and cause fracture of the viscoelastic gel membrane. For simplicity, the fracture process is not considered in the current model. The model prediction agrees with the experimental observations and confirms our hypothesis. The final retraction in the growth curves in Figure 9 is caused by the artificial elasticity because of the selection of the reference state, as discussed above.

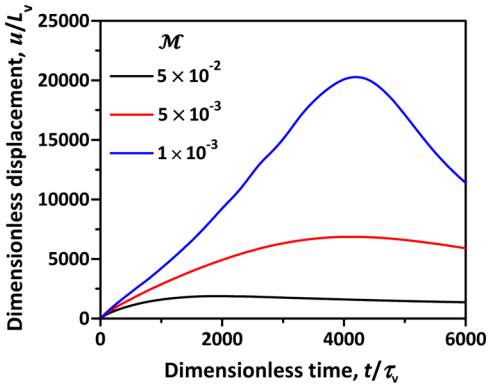

Figure 9. Dimensionless radial displacement of the edge of the solution drop during the spreading process, u/L_v, at various values of the dimensionless parameter $\mathcal{M} = \mu_0\eta D/\Delta\gamma^2$.

CONCLUSIONS

In summary, we have investigated the spreading and gelation processes of the ethanol solutions of P(SA-*co*-AAc) to prepare hydrogel films after being dripped onto water surface. The spreading was blocked when C_P was too high, whereas the film was fragmented into small pieces when C_P was too low. At intermediate C_P values, continuous hydrogel films were obtained. By incorporating AIE fluorogens, we found that the spreading proceeded ahead of the gelation process. Steady spreading was observed during the formation of uniform hydrogel films, in which the differential surface tension between water and ethanol as the driven force was balanced with the viscous stress of the polymer solution and the elastic stress from the thin gel membrane at the solution−water interface. The spreading speed decreased with the increase in f and C_P, which led to an increase in the viscosity and surface tension of the ethanol solution. The spreading speed was found to scale with the ratio between the differential surface tension and the solution viscosity. The steadiness of the spreading and the uniformity of the resulting gel film, on the other hand, were guaranteed by the elasticity of the thin gel membrane formed on the solution−water interface earlier in the process. This work provided a general understanding of the detailed process and governing kinetics of the Marangoni effect-assisted preparation of hydrogel films. The principle should be applicable to other systems with different polymers and solvents at different temperatures, so as to prepare thin supramolecular gel films with versatile functions.

ASSOCIATED CONTENT

Supporting Information

The Supporting Information is available free of charge on the ACS Publications website at DOI: 10.1021/acs.langmuir.8b02626.

Viscosity of the ethanol solution of P(SA-*co*-AAc) over a wide range of shear rate at room temperature and with different f and C_P as a function of the shear rate at room temperature (PDF)

AUTHOR INFORMATION

Corresponding Authors

*E-mail: wuziliang@zju.edu.cn (Z.L.W.).
*E-mail: hongw@sustc.edu.cn (W.H.).

ORCID

Pengju Pan: 0000-0001-6924-5485
Jing Zhi Sun: 0000-0001-5478-5841
Zi Liang Wu: 0000-0002-1824-9563

Notes

The authors declare no competing financial interest.

DOI: 10.1021/acs.langmuir.8b02626
Langmuir 2018, 34, 12310−12317

■ ACKNOWLEDGMENTS

This work was supported by the National Natural Science Foundation of China (51773179) and Thousand Young Talents Program of China.

■ REFERENCES

(1) Zhao, K.; Zhang, X.; Wei, J.; Li, J.; Zhou, X.; Liu, D.; Liu, Z.; Li, J. Calcium Alginate Hydrogel Filtration Membrane with Excellent Anti-Fouling Property and Controlled Separation Performance. *J. Membr. Sci.* **2015**, *492*, 536−546.

(2) Kumar, P. T. S.; Lakshmanan, V.-K.; Anilkumar, T. V.; Ramya, C.; Reshmi, P.; Unnikrishnan, A. G.; Nair, S. V.; Jayakumar, R. Flexible and Microporous Chitosan Hydrogel/Nano ZnO Composite Bandages for Wound Dressing: in vitro and in vivo Evaluation. *ACS Appl. Mater. Interfaces* **2012**, *4*, 2618−2629.

(3) Ionov, L. Biomimetic Hydrogel-Based Actuating Systems. *Adv. Funct. Mater.* **2013**, *23*, 4555−4570.

(4) Wang, K.; Zhang, X.; Li, C.; Sun, X.; Meng, Q.; Ma, Y.; Wei, Z. Chemically Crosslinked Hydrogel Film Leads to Integrated Flexible Supercapacitors with Superior Performance. *Adv. Mater.* **2015**, *27*, 7451−7457.

(5) Matsukuma, D.; Yamamoto, K.; Aoyagi, T. Stimuli-Responsive Properties ofN-Isopropylacrylamide-Based Ultrathin Hydrogel Films Prepared by Photo-Cross-Linking. *Langmuir* **2006**, *22*, 5911−5915.

(6) Goujon, L. J.; Hariharan, S.; Sayyar, B.; Burke, N. A. D.; Cranston, E. D.; Andrews, D. W.; Stöver, H. D. H. Tunable Hydrogel Thin Films from Reactive Synthetic Polymers as Potential Two-Dimensional Cell Scaffolds. *Langmuir* **2015**, *31*, 5623−5632.

(7) Zhang, Y.; Ionov, L. Reversibly Cross-Linkable Thermoresponsive Self-Folding Hydrogel Films. *Langmuir* **2015**, *31*, 4552−4557.

(8) Calvert, P. Hydrogels for Soft Machines. *Adv. Mater.* **2009**, *21*, 743−756.

(9) Zhao, X. Multi-Scale Multi-Mechanism Design of Tough Hydrogels: Building Dissipation into Stretchy Networks. *Soft Matter* **2014**, *10*, 672−687.

(10) Wang, W.; Zhang, Y.; Liu, W. Bioinspired Fabrication of High Strength Hydrogels from Non-Covalent Interactions. *Prog. Polym. Sci.* **2017**, *71*, 1−25.

(11) Zhang, Y. S.; Khademhosseini, A. Advances in Engineering hydrogels. *Science* **2017**, *356*, eaaf3627.

(12) Liang, S.; Yu, Q. M.; Yin, H.; Wu, Z. L.; Kurokawa, T.; Gong, J. P. Ultrathin Tough Double Network Hydrogels Showing Adjustable Muscle-Like Isometric Force Generation Triggered by Solvent. *Chem. Commun.* **2009**, *48*, 7518−7520.

(13) Liang, S.; Wu, Z. L.; Hu, J.; Kurokawa, T.; Yu, Q. M.; Gong, J. P. Direct Observation on the Surface Fracture of Ultrathin Film Double-Network Hydrogels. *Macromolecules* **2011**, *44*, 3016−3020.

(14) Henderson, K. J.; Zhou, T. C.; Otim, K. J.; Shull, K. R. Ionically Cross-Linked Triblock Copolymer Hydrogels with High Strength. *Macromolecules* **2010**, *43*, 6193−6201.

(15) Naficy, S.; Spinks, G. M.; Wallace, G. G. Thin, Tough, pH-Sensitive Hydrogel Films with Rapid Load Recovery. *ACS Appl. Mater. Interfaces* **2014**, *6*, 4109−4114.

(16) Zheng, S. Y.; Ding, H.; Qian, J.; Yin, J.; Wu, Z. L.; Song, Y.; Zheng, Q. Metal-Coordination Complexes Mediated Physical Hydrogels with High Toughness, Stick-Slip Tearing Behavior, and Good Processability. *Macromolecules* **2016**, *49*, 9637−9646.

(17) Yu, H. C.; Zhang, H.; Ren, K.; Ying, Z.; Zhu, F.; Qian, J.; Ji, J.; Wu, Z. L.; Zheng, Q. Ultrathin κ-Carrageenan/Chitosan Hydrogel Films with High Toughness and Antiadhesion Property. *ACS Appl. Mater. Interfaces* **2018**, *10*, 9002−9009.

(18) Tian, Y.; Wei, X.; Wang, Z. J.; Pan, P.; Li, F.; Ling, D.; Wu, Z. L.; Zheng, Q. A Facile Approach to Prepare Tough and Responsive Ultrathin Physical Hydrogel Films as Artificial Muscles. *ACS Appl. Mater. Interfaces* **2017**, *9*, 34349−34355.

(19) Matsuda, A.; Sato, J.; Yasunaga, H.; Osada, Y. Order-Disorder Transition of a Hydrogel Containing an n-alkyl acrylate. *Macromolecules* **1994**, *27*, 7695−7698.

(20) Geng, Y.; Lin, X. Y.; Pan, P.; Shan, G.; Bao, Y.; Song, Y.; Wu, Z. L.; Zheng, Q. Hydrophobic Association Mediated Physical Hydrogels with High Strength and Healing Ability. *Polymer* **2016**, *100*, 60−68.

(21) Zhang, Y.; Chen, G.; Lin, Y.; Zhao, L.; Yuan, W. Z.; Lu, P.; Jim, C. K. W.; Zhang, Y.; Tang, B. Z. Thiol-bromo click polymerization for multifunctional polymers: synthesis, light refraction, aggregation-induced emission and explosive detection. *Polym. Chem.* **2015**, *6*, 97−105.

(22) Ahuja, A.; Taylor, J. A.; Lifton, V.; Sidorenko, A. A.; Salamon, T. R.; Lobaton, E. J.; Kolodner, P.; Krupenkin, T. N. Nanonails: A Simple Geometrical Approach to Electrically Tunable Superlyophobic Surfaces. *Langmuir* **2008**, *24*, 9−14.

(23) Wang, Y.; Liu, X.; Li, X.; Wu, J.; Long, Y.; Zhao, N.; Xu, J. Directional and Path-Finding Motion of Polymer Hydrogels Driven by Liquid Mixing. *Langmuir* **2012**, *28*, 11276−11280.

(24) Scriven, L. E.; Sternling, C. V. The Marangoni Effects. *Nature* **1960**, *187*, 186−188.

(25) Pimienta, V.; Antoine, C. Self-Propulsion on Liquid Surfaces. *Curr. Opin. Colloid Interface Sci.* **2014**, *19*, 290−299.

(26) Gong, J. P.; Matsumoto, S.; Uchida, M.; Isogai, N.; Osada, Y. Motion of Polymer Gels by Spreading Organic Fluid on Water. *J. Phys. Chem.* **1996**, *100*, 11092−11097.

(27) Mitsumata, T.; Ikeda, K.; Gong, J. P.; Osada, Y. Solvent-Driven Chemical Motor. *Appl. Phys. Lett.* **1998**, *73*, 2366−2368.

(28) Mitsumata, T.; Ikeda, K.; Gong, J. P.; Osada, Y. Controlled Motion of Solvent-Driven Gel Motor and Its Application as a Generator. *Langmuir* **2000**, *16*, 307−312.

(29) Bassik, N.; Abebe, B. T.; Gracias, D. H. Solvent Driven Motion of Lithographically Fabricated Gels. *Langmuir* **2008**, *24*, 12158−12163.

(30) Sharma, R.; Chang, S. T.; Velev, O. D. Gel-Based Self-Propelling Particles Get Programmed to Dance. *Langmuir* **2012**, *28*, 10128−10135.

(31) Wang, L.; Yuan, B.; Lu, J.; Tan, S.; Liu, F.; Yu, L.; He, Z.; Liu, J. Self-Propelled and Long-Time Transport Motion of PVC Particles on a Water Surface. *Adv. Mater.* **2016**, *28*, 4065−4070.

(32) Yasunaga, H.; Ando, I. Dynamic behavior of water in hydro-swollen crosslinked polymer gel as studied by PGSE 1H NMR and pulse 1H NMR. *Polym. Gels Networks* **1993**, *1*, 83−92.

(33) Wang, Z. J.; Hong, W.; Wu, Z. L.; Zheng, Q. Site-Specific Pre-Swelling-Directed Morphing Structures of Patterned Hydrogels. *Angew. Chem., Int. Ed.* **2017**, *56*, 15974−15978.

(34) Mei, J.; Leung, N. L. C.; Kwok, R. T. K.; Lam, J. W. Y.; Tang, B. Z. Aggregation-Induced Emission: Together We Shine, United We Soar! *Chem. Rev.* **2015**, *115*, 11718−11940.

(35) Wang, Z.; Nie, J.; Qin, W.; Hu, Q.; Tang, B. Z. Gelation Process Visualized by Aggregation-Induced Emission Fluorogens. *Nat. Commun.* **2016**, *7*, 12033.

(36) Carreau, P. J. *Rheology of Polymeric Systems: Principles and Applications*; Hanser Publishers: Munich, 1997.

(37) Suematsu, N. J.; Sasaki, T.; Nakata, S.; Kitahata, H. Quantitative Estimation of the Parameters for Self-Motion Driven by Difference in Surface Tension. *Langmuir* **2014**, *30*, 8101−8108.

(38) Suciu, D. G.; Smigelschi, O.; Ruckenstein, E. Some Experiments on the Marangoni Effect. *AIChE J.* **1967**, *13*, 1120−1124.

(39) Joos, P.; Pintens, J. Spreading Kinetics of Liquids on Liquids. *J. Colloid Interface Sci.* **1977**, *60*, 507−513.

(40) Svitova, T. F.; Hill, R. M.; Radke, C. J. Spreading of Aqueous Dimethyldidodecylammonium Bromide Surfactant Droplets over Liquid Hydrocarbon Substrates. *Langmuir* **1999**, *15*, 7392−7402.

(41) Svitova, T. F.; Hill, R. M.; Radke, C. J. Spreading of Aqueous Trisiloxane Surfactant Solutions over Liquid Hydrophobic Substrates. *Langmuir* **2001**, *17*, 335−348.

(42) Berg, S. Marangoni-Driven Spreading along Liquid-Liquid Interfaces. *Phys. Fluids* **2009**, *21*, 032105.

(43) Hu, H.; Larson, R. G. Analysis of the Effects of Marangoni Stresses on the Microflow in an Evaporating Sessile Droplet. *Langmuir* **2005**, *21*, 3972−3980.

DOI: 10.1021/acs.langmuir.8b02626
Langmuir 2018, 34, 12310−12317